Journal of Computational Physics 443 (2021) 110530

Contents lists available at ScienceDirect

Journal of Computational Physics

www.elsevier.com/locate/jcp

High-order finite difference method for the Schrödinger equation on deforming domains

Ylva Ljungberg Rydin [a,*], Ken Mattsson [a], Jonatan Werpers [a], Erik Sjöqvist [b]

[a] Department of Information Technology, Uppsala University, Lägerhyddsvägen 2, Se-752 37 Uppsala, Sweden
[b] Department of Physics and Astronomy, Uppsala University, Box 516, Se-751 20 Uppsala, Sweden

ARTICLE INFO

Article history:
Available online 24 June 2021

Keywords:
Finite difference methods
Quantum mechanics
High-order accuracy
Stability
Boundary treatment
Deforming domain

ABSTRACT

A high-order finite difference discretisation of the Schrödinger equation on domains that deform in time is presented. For the domain deformation, a time-dependent coordinate transformation is used. The utilisation of *summation-by-parts* finite difference operators, combined with boundary conditions imposed weakly by a penalty technique, leads to a provably stable scheme. The convergence properties of the scheme are verified by numerical computations. The capabilities of the numerical scheme are demonstrated by simulations of Berry phases in deforming quantum billiards.

1. Introduction

Particles localised in two-dimensional (2D) spatial domains surrounded by infinite potential walls is a much used model in the study of quantum chaos [1]. The energy levels of such model systems typically show a rich behaviour of avoided crossings and crossings occurring in domains that lack symmetry ('diabolical points') [2]. The corresponding wave functions show complex structures, such as 'scars' resembling classical periodic orbits [3] and non-trivial Berry phases when adiabatically deforming the domain around a crossing point [4]. To study such systems there is a need for numerical methods that can efficiently solve the Schrödinger equation on time-dependent domains. Because the deformation of the domain and the wave function often exhibit different timescales these methods must be able to provide long time simulation without loss of accuracy. In this article, we derive a stable and accurate high-order *summation-by-parts* (SBP) finite difference scheme for the 2D Schrödinger equation on deforming domains that can be used to efficiently model this type of complex quantum systems.

Solutions of the Schrödinger equation are in general wave dominated; therefore numerical methods with low dispersion errors are needed for efficient numerical solutions. It is well known that higher-order finite difference methods are well suited for this type of problem. However, constructing stable boundary treatment for these methods is a non-trivial task, which has received considerable attention in the past, see e.g. [5–9].

A technique for constructing stable high-order finite difference methods for initial-boundary-value-problems is to combine discretisation with SBP finite difference operators with a weak method of imposing the boundary conditions, *simultaneous-approximation-term* (SAT). Details on the SBP-SAT technique are given in Section 3 and thorough reviews of the methodology can be found in [10,11]. The SBP-SAT technique has been extended to the time-dependent Schrödinger equation on fixed domains by Nissen *et al.* in [12,13], but so far the development of the SBP-SAT technique has been mainly focused on problems on fixed domains. How to extend the technique to deforming domains for first order hyper-

* Corresponding author.
E-mail address: ylva.rydin@it.uu.se (Y. Ljungberg Rydin).

https://doi.org/10.1016/j.jcp.2021.110530

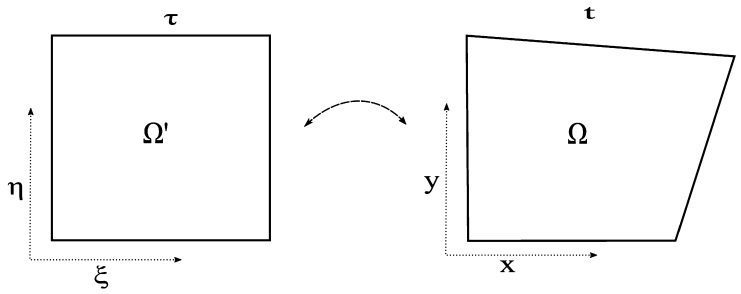

Fig. 1. Coordinate transformation between the physical domain Ω and the computational domain Ω'.

bolic systems by a time-dependent coordinate transformation is described in [14]. In this article we apply and extend these techniques for the 2D Schrödinger equation.

This article is organised as follows. In Sec. 2, the continuous problem is transformed by a time-dependent coordinate transformation. In Sec. 3, the SBP method is introduced and a spatial discretisation of the transformed equation is presented. Sec. 4 contains a convergence study on the numerical scheme and in Sec. 5 numerical simulations reproducing physical experiments of adiabatic evolution and associated Berry phases in quantum billiard are presented. Sec. 6 summarises and concludes the work.

2. Continuous analysis

We consider the Schrödinger equation for a single particle in two space dimensions. The infinite potential walls are described using Dirichlet boundary conditions. While we limit the analysis to 2D the methodology can be extended to higher dimensions in a straightforward manner. For a particle in a time-dependent domain $\Omega(t)$ with wave function $\hat{u} = \hat{u}(t, x, y)$ we have

$$\begin{aligned} &\hat{u}_t = i\Delta\hat{u} - iV(x, y, t)\hat{u}, && t > t_0, && (x, y) \in \Omega(t), \\ &\hat{u} = 0, && t \geq t_0, && (x, y) \in \partial\Omega(t), \\ &\hat{u} = \hat{u}_0(x, y), && t = t_0, && (x, y) \in \Omega(t). \end{aligned} \tag{1}$$

Here, $\partial\Omega(t)$ denotes the domain boundary and $\hat{u}_0$ the initial wave function of the particle.

To allow for discretisation using finite differences, we apply a time-dependent coordinate transformation to map the physical deforming domain $\Omega(t)$ to a static Cartesian domain Ω' according to Fig. 1. From here on, the mapping is assumed to be one-to-one. Denote the mapping by

$$\begin{aligned} &x = x(\xi, \eta, \tau), \quad y = y(\xi, \eta, \tau), \quad t = t(\tau), \\ &\xi = \xi(x, y, t), \quad \eta = \eta(x, y, t), \quad \tau = \tau(t). \end{aligned} \tag{2}$$

In the following, metrical properties that let us rewrite the Schrödinger equation (1) in terms of ξ, η and τ are presented. The coordinate transformation has the Jacobian determinant

$$J = \begin{vmatrix} x_\xi & x_\eta & x_\tau \\ y_\xi & y_\eta & y_\tau \\ 0 & 0 & 1 \end{vmatrix} = x_\xi y_\eta - x_\eta y_\xi, \tag{3}$$

where we have used that $t_\xi = t_\eta = 0$ and $t_\tau = 1$. Since the transformation is one-to-one, the metric relations

$$\begin{aligned} &\xi_x = \frac{y_\eta}{J}, \quad \xi_y = -\frac{x_\eta}{J}, \quad \xi_t = \frac{x_n y_\tau - x_\tau y_n}{J}, \\ &\eta_x = -\frac{y_\xi}{J}, \quad \eta_y = \frac{x_\xi}{J}, \quad \eta_t = \frac{x_\tau y_\xi - x_\xi y_\tau}{J}, \end{aligned} \tag{4}$$

can be derived by the inverse function theorem. These relations allow us to rewrite the time derivative as

$$J\frac{\partial}{\partial t} = J\frac{\partial}{\partial \tau}\tau_t + J\frac{\partial}{\partial \xi}\xi_t + J\frac{\partial}{\partial \eta}\eta_t = J\frac{\partial}{\partial \tau} + \gamma_1\frac{\partial}{\partial \xi} + \gamma_2\frac{\partial}{\partial \eta}. \tag{5}$$

Here, $\gamma_1 = x_\eta y_\tau - x_\tau y_\eta$ and $\gamma_2 = x_\tau y_\xi - x_\xi y_\tau$. As shown in [15] the Laplace operator on some function v in curvilinear coordinates is

$$\Delta v = \frac{1}{J}\big[(\alpha_1 v_\xi)_\xi + (\beta v_\eta)_\xi + (\beta v_\xi)_\eta + (\alpha_2 v_\eta)_\eta\big], \tag{6}$$

where

$$\alpha_1 = \frac{1}{J}(x_\eta^2 + y_\eta^2) \quad \alpha_2 = \frac{1}{J}(x_\xi^2 + y_\xi^2), \quad \beta = -\frac{1}{J}(x_\eta x_\xi + y_\eta y_\xi). \tag{7}$$

Hence, the Schrödinger equation (1) for the wave function $u = u(\tau, \xi, \eta) = \hat{u}(t(\tau), x(\xi, \eta, \tau), y(\xi, \eta, \tau))$ can be written in the new coordinates on the Cartesian static domain as

$$\begin{aligned} &u_\tau + \tfrac{1}{J}(\gamma_1 u_\xi + \gamma_2 u_\eta) = i\Delta u - iV(\xi, \eta, \tau)u, && \tau > \tau_0, \quad (\xi, \eta) \in \Omega', \\ &u = 0, && \tau \geq \tau_0, \quad (\xi, \eta) \in \partial\Omega', \\ &u = u_0(\xi, \eta) && \tau = \tau_0, \quad (\xi, \eta) \in \Omega'. \end{aligned} \tag{8}$$

By using the chain rule, the left-hand side can be rewritten as

$$\begin{aligned} u_\tau + \frac{1}{J}(\gamma_1 u_\xi + \gamma_2 u_\eta) = u_\tau + \frac{1}{2J}\big[&\gamma_1 u_\xi + (\gamma_1 u)_\xi - \gamma_{1\xi} u + \\ &+ \gamma_2 u_\eta + (\gamma_2 u)_\eta - \gamma_{2\eta} u\big]. \end{aligned} \tag{9}$$

The relation $J_\tau + \gamma_{1\xi} + \gamma_{2\eta} = 0$, which follows from the metric relations in Eq. (4), combined with Eq. (9) results in

$$u_\tau = -\mathcal{T}(u) + i\Delta u - iV(\xi, \eta, \tau)u, \tag{10}$$

where $\mathcal{T}(u) = \frac{1}{2J}\big[\gamma_1 u_\xi + (\gamma_1 u)_\xi + \gamma_2 u_\eta + (\gamma_2 u)_\eta - J_\tau u\big]$. This is the form of the Schrödinger equation that is discretised in Sec. 3.

The Schrödinger equation is known to be wellposed and we could conclude this section here. However, the derivation of the continuous energy estimate is the template and guide for our proof of stability for the numerical scheme in Sec. 3. Therefore, we present it below.

Let $(v, w)_\Omega = \int_\Omega v^* w \, dxdy = \int_{\Omega'} v^* J w \, d\xi d\eta$ and $(v, w)_{\Omega'} = \int_{\Omega'} v^* w \, d\xi d\eta$ be the inner products with the corresponding norms $\|v\|_\Omega^2 = (v, v)_\Omega$ and $\|v\|_{\Omega'}^2 = (v, v)_{\Omega'}$. Here v^* denotes the complex conjugate of v. A mathematical energy for the Schrödinger equation is the total probability of the wave function. For a wave function u the total probability is $\|u\|_\Omega^2 = 1$ and preservation is equivalent to $\frac{d}{d\tau}\|u\|_\Omega^2 = 0$. To show this, expand the left hand side by the product rule,

$$\begin{aligned} \frac{d}{d\tau}\|u\|_\Omega^2 &= (u_\tau, u)_\Omega + (u, u_\tau)_\Omega + (u, J_\tau u)_{\Omega'} \\ &= 2\,\mathrm{Re}[(u, u_\tau)_\Omega] + (u, J_\tau u)_{\Omega'}. \end{aligned} \tag{11}$$

Note that $(u_\tau, u)_\Omega$ is the complex conjugate of $(u, u_\tau)_\Omega$, hence $(u_\tau, u)_\Omega + (u, u_\tau)_\Omega = 2\,\mathrm{Re}[(u, u_\tau)_\Omega]$. Taking the inner product of u and the Schrödinger equation (10) gives

$$(u, u_\tau)_\Omega = -(u, \mathcal{T}(u))_\Omega - i(u, \Delta u)_{\Omega'} - i(u, V(\xi, \eta, \tau)u)_{\Omega'} \tag{12}$$

which has the real part

$$\mathrm{Re}[(u, u_\tau)_\Omega] = -\,\mathrm{Re}[(u, \mathcal{T}(u))_\Omega] + \mathrm{Im}[(u, \Delta u)_\Omega]. \tag{13}$$

Using *integration-by-parts* it is straightforward to show that $\mathrm{Re}[(u, \mathcal{T}(u))_\Omega] = \frac{1}{2}(u, J_\tau u)_{\Omega'}$ and $\mathrm{Im}[(u, \Delta u)_\Omega] = 0$. Hence, $\frac{d}{d\tau}\|u\|_\Omega^2 = 0$.

3. Discretisation

In this section, we discretise the transformed Schrödinger equation (10). Before presenting the discretisation, the SBP finite difference operators and some necessary notation is introduced.

The computational domain Ω' is discretised on the $(N_\xi + 1) \times (N_\eta + 1)$ grid points

$$\xi_{ij} = \frac{i}{N_\xi}, \quad \eta_{ij} = \frac{j}{N_\eta}, \quad i = 0, 1, \ldots, N_\xi, \quad j = 0, 1, \ldots, N_\eta. \tag{14}$$

Any function a evaluated at a grid point is denoted a_{ij} and it is represented on the grid by the vector

$$\bar{a} = [a_{00}, a_{01}, \ldots, a_{0N_\eta}, a_{10}, \ldots, a_{N_\xi N_\eta}]^\top. \tag{15}$$

Further, $\bar{\bar{a}}$ denotes a diagonal matrix with the vector $\bar{a}$ on the diagonal. The approximate solution to (10) is represented by the vector $\bar{u}$. As in the continuous case, we define two discrete inner products. For vectors $\bar{v}, \bar{w} \in \mathbb{C}^{(N_\xi+1)\times(N_\eta+1)}$, let $(\bar{v}, \bar{w})_{\bar{\Omega}} = \bar{v}^* H \bar{\bar{J}} \bar{w}$ and $(\bar{v}, \bar{w})_{\bar{\Omega}'} = \bar{v}^* H \bar{w}$ be discrete inner products with the corresponding norms $\|\bar{v}\|_{\bar{\Omega}}^2 = (\bar{v}, \bar{v})_{\bar{\Omega}}$ and $\|\bar{v}\|_{\bar{\Omega}'}^2 = (\bar{v}, \bar{v})_{\bar{\Omega}'}$. Here, $\bar{v}^*$ denotes the conjugate transpose of $\bar{v}$. The matrix H is diagonal, positive definite, and related to the SBP operators. In the following analysis, the four domain boundaries are denoted $\mathcal{W}$ (west at $\xi = 0$), $\mathcal{E}$ (east at $\xi = 1$), $\mathcal{S}$ (south at $\eta = 0$), and $\mathcal{N}$ (north at $\eta = 1$).

3.1. Summation-by-parts finite differences

The SBP-operators used in this paper are the narrow-stencil finite difference operators first introduced in [16]. These operators are high-order central finite difference operators constructed to mimic the continuous *integration-by-parts* property by the discrete SBP property. In the one-dimensional case, the first derivative in ξ is approximated by SBP-operators as

$$u_\xi = D_1 \bar{u} + \bar{T}, \tag{16}$$

where $\bar{T}$ is the truncation error. The second derivative with a variable coefficient b is approximated by

$$(bu_\xi)_\xi = D_2^{(\bar{b})} \bar{u} + \bar{T}. \tag{17}$$

These operators satisfy the SBP properties for the first and second derivative, which means that

$$(\bar{u}, D_1 \bar{v})_{\bar{\Omega}'_\xi} = u^*_{N_\xi} v_{N_\xi} - u^*_1 v_1 - (D_1 \bar{u}, \bar{v})_{\bar{\Omega}'_\xi}, \tag{18}$$

and

$$(\bar{u}, D_2^{(\bar{b})} \bar{v})_{\bar{\Omega}'_\xi} = u^*_{N_\xi} b_{N_\xi} d^\top_{N_\xi} \bar{v} - u^*_1 b_1 d_1^\top \bar{v} - \bar{u}^* M^{(\bar{b})} \bar{v}. \tag{19}$$

Here, the one-dimensional domain Ω'_ξ is the real line between $\xi = 0$ and $\xi = 1$. Further, $d_1^\top \bar{v} = v_{\xi 1} + T_1$ at $\xi = 0$ and $d^\top_{N_\xi} \bar{v} = v_{\xi N_\xi} + T_{N_\xi}$ at $\xi = 1$. $M^{(\bar{b})}$ is a positive semi-definite matrix.

Remark 1. The truncation error $\bar{T}$ for a *pth* order operator is of order h^p in the interior stencil and $h^{p/2}$ at a few points near the boundary [16]. While the order is lower at the boundary, it is important to keep in mind that the boundary accuracy alone does not dictate the convergence rate when solving partial differential equations. The expected global convergence rate can actually be shown to be higher. In [17], it is shown that a point-wise stable approximation of an initial-boundary-value-problem involving derivatives up to order q yields a convergence rate of order $k = \min(p, q + p/2)$. Hence the rate $k = \min(p, 2 + p/2)$ is expected when solving the Schrödinger equation. As an example, the 6*th* order SBP operators have $p = 6$, which gives the expected convergence rate $k = 5$.

The one-dimensional SBP operators are extended to two dimensions by the Kronecker tensor product denoted $\otimes$. For notational simplicity we assume $N_\xi = N_\eta = N$ in the following analysis. This simplification does not restrict the generality of the method. The spatial step is $h = 1/N$ in both dimensions. Let I_m denote the $m \times m$ unit matrix and let the vectors $e_1, e_2, ..., e_m$ be the columns of I_m and $E_{(k)} = e_k \otimes e_k$. Using this, we introduce the difference operators

$$D_{1\xi} = D_1 \otimes I_N, \qquad D_{1\eta} = I_N \otimes D_1,$$

$$D_{2\xi}^{(\bar{b})} = \sum_{k=1}^{N} D_2^{(\bar{b}(\xi,\eta_k))} \otimes E_{(k)}, \quad D_{2\eta}^{(\bar{b})} = \sum_{k=1}^{N} E_{(k)} \otimes D_2^{(\bar{b}(\xi_k,\eta))},$$

the matrices,

$$M_\xi = M \otimes I_N, \quad M_\eta = I_N \otimes M,$$

and a matrix defining a discrete inner product for the domain,

$$H_{\xi\eta} = H \otimes H.$$

Further, we construct matrices that select the boundary elements

$$e_{\mathcal{W}} = I_N \otimes e_1, \quad e_{\mathcal{E}} = I_N \otimes e_N, \quad e_{\mathcal{S}} = e_1 \otimes I_N, \quad e_{\mathcal{N}} = e_N \otimes I_N,$$

and d_1 and d_N are extended as

$$d_{\mathcal{W}} = I_N \otimes d_1, \quad d_{\mathcal{E}} = I_N \otimes d_N, \quad d_{\mathcal{S}} = d_1 \otimes I_N, \quad d_{\mathcal{N}} = d_N \otimes I_N.$$

For any grid function $\bar{v}$, let

$$\bar{v}_{(\mathcal{W})} = e_{\mathcal{W}}^\top \bar{v}, \quad \bar{v}_{(\mathcal{E})} = e_{\mathcal{E}}^\top \bar{v}, \quad \bar{v}_{(\mathcal{S})} = e_{\mathcal{S}}^\top \bar{v}, \quad \bar{v}_{(\mathcal{N})} = e_{\mathcal{N}}^\top \bar{v}.$$

3.2. Spatial discretisation

Discretising the transformed Schrödinger equation (10) in space with the above operators and SAT gives

$$\bar{u}_\tau = -D_{\mathcal{T}}\bar{u} + iD_\Delta\bar{u} - i\bar{\bar{V}}\bar{u} + SAT_\Delta + SAT_{\mathcal{T}}, \tag{20}$$

where

$$D_{\mathcal{T}} = \bar{\bar{J}}^{-1}(\bar{\bar{\gamma}}_1 D_{1\xi} + D_{1\xi}\bar{\bar{\gamma}}_1 + \bar{\bar{\gamma}}_2 D_{1\eta} + D_{1\eta}\bar{\bar{\gamma}}_2 - \bar{\bar{J}}_\tau)/2, \tag{21}$$

is the discretisation of $\mathcal{T}$ and

$$D_\Delta = \bar{\bar{J}}^{-1}(D_{2\xi}^{(\bar{\alpha}_1)} + D_{1\xi}\bar{\bar{\beta}}D_{1\eta} + D_{1\eta}\bar{\bar{\beta}}D_{1\xi} + D_{2\eta}^{(\bar{\alpha}_2)}), \tag{22}$$

the discrete Laplace operator.

For a stable scheme, that preserves the discrete probability $\|\bar{u}\|_{\bar{\Omega}}$ the SAT-terms are chosen as:

$$\begin{aligned} 2SAT_{\mathcal{T}} = {} & \bar{\bar{J}}^{-1}H_{\xi\eta}^{-1}e_{\mathcal{W}}H\bar{\bar{\gamma}}_1 e_{\mathcal{W}}^\top\bar{u} - \bar{\bar{J}}^{-1}H_{\xi\eta}^{-1}e_{\mathcal{E}}H\bar{\bar{\gamma}}_1 e_{\mathcal{E}}^\top\bar{u} \\ & + \bar{\bar{J}}^{-1}H_{\xi\eta}^{-1}e_{\mathcal{S}}H\bar{\bar{\gamma}}_2 e_{\mathcal{S}}^\top\bar{u} - \bar{\bar{J}}^{-1}H_{\xi\eta}^{-1}e_{\mathcal{N}}H\bar{\bar{\gamma}}_2 e_{\mathcal{N}}^\top\bar{u} \end{aligned} \tag{23}$$

and

$$\begin{aligned} SAT_\Delta = {} & \bar{\bar{J}}^{-1}H_{\xi\eta}^{-1}(d_{\mathcal{W}}\bar{\bar{\alpha}}_1 + D_{1\eta}^\top e_{\mathcal{W}}\bar{\bar{\beta}})He_{We}^\top\bar{u} \\ & - \bar{\bar{J}}^{-1}H_{\xi\eta}^{-1}(d_{\mathcal{E}}\bar{\bar{\alpha}}_1 + D_{1\eta}^\top e_{\mathcal{E}}\bar{\bar{\beta}})He_{ea}^\top\bar{u} \\ & + \bar{\bar{J}}^{-1}H_{\xi\eta}^{-1}(d_{\mathcal{S}}\bar{\bar{\alpha}}_2 + D_{1\xi}^\top e_{\mathcal{S}}\bar{\bar{\beta}})He_{\mathcal{S}}^\top\bar{u} \\ & - \bar{\bar{J}}^{-1}H_{\xi\eta}^{-1}(d_{\mathcal{N}}\bar{\bar{\alpha}}_2 + D_{1\xi}^\top e_{\mathcal{N}}\bar{\bar{\beta}})He_{\mathcal{N}}^\top\bar{u}. \end{aligned} \tag{24}$$

Theorem 1. *The semi-discrete problem* (20) *is time-stable if the SAT-terms are chosen as* (23) *and* (24).

Proof. If we show that the scheme preserves the discrete probability density the scheme is time-stable. As in the continuous case the probability density is preserved if $\frac{d}{d\tau}\|\bar{u}\|_{\bar{\Omega}}^2 = 0$. Multiplying (20) from the left by $\bar{u}H\bar{\bar{J}}$ gives

$$\frac{d}{d\tau}\|\bar{u}\|_{\bar{\Omega}}^2 = -2\,\mathrm{Re}[(\bar{u}, D_{\mathcal{T}}\bar{u} + SAT_{\mathcal{T}})_{\bar{\Omega}}] + 2\,\mathrm{Im}[(\bar{u}, D_\Delta\bar{u} + SAT_\Delta)_{\bar{\Omega}}] + (\bar{u}, \bar{\bar{J}}_\tau\bar{u})_{\bar{\Omega}'}. \tag{25}$$

We start by treating first term of the left hand side of (25), related to $D_{\mathcal{T}}$: As in the continuous case, the aim is to show that this term cancels $(\bar{u}, \bar{\bar{J}}_\tau\bar{u})_{\bar{\Omega}'}$. By the SBP property, in (18), which is the discrete equivalent of the *integration-by-parts* property that was applied in the continuous analysis, we get

$$(\bar{u}, \bar{\bar{\gamma}}_1 D_{1\xi}\bar{u})_{\bar{\Omega}'} = -(D_{1\xi}\bar{\bar{\gamma}}_1\bar{u}, \bar{u})_{\bar{\Omega}'} + BT_\xi, \tag{26}$$

and

$$(\bar{u}, \bar{\bar{\gamma}}_2 D_{1\eta}\bar{u})_{\bar{\Omega}'} = -(D_{1\eta}\bar{\bar{\gamma}}_2\bar{u}, \bar{u})_{\bar{\Omega}'} + BT_\eta. \tag{27}$$

Here, the boundary terms are

$$\begin{aligned} BT_\xi &= \bar{u}_{(\mathcal{E})}^* H\bar{\bar{\gamma}}_1\bar{u}_{(\mathcal{E})} - \bar{u}_{(\mathcal{W})}^* H_\eta\bar{\bar{\gamma}}_1\bar{u}_{(\mathcal{W})}, \\ BT_\eta &= \bar{u}_{(\mathcal{N})}^* H\bar{\bar{\gamma}}_2\bar{u}_{(\mathcal{N})} - \bar{u}_{(\mathcal{S})}^* H_\xi\bar{\bar{\gamma}}_2\bar{u}_{(\mathcal{S})}. \end{aligned} \tag{28}$$

Since $(\bar{u}, \bar{\bar{\gamma}}_1 D_\xi\bar{u})_{\bar{\Omega}'} = (D_\xi\bar{\bar{\gamma}}_1\bar{u}, \bar{u})_{\bar{\Omega}'}^*$, the first parenthesis in (25) can be written as

$$\mathrm{Re}[(\bar{u}, D_{\mathcal{T}}\bar{u} + SAT_{\mathcal{T}})_{\bar{\Omega}}] = \mathrm{Re}[(\bar{u}, SAT_{\mathcal{T}})_{\bar{\Omega}} + \frac{1}{2}BT_\xi + \frac{1}{2}BT_\eta] - \frac{1}{2}(\bar{u}, \bar{\bar{J}}_\tau\bar{u})_{\bar{\Omega}'}. \tag{29}$$

Inserting the SAT_τ defined in (23) yields

$$2\,\mathrm{Re}[(\bar{u}, D_{\mathcal{T}}\bar{u} + SAT_{\mathcal{T}})_{\bar{\Omega}}] = -(\bar{u}, \bar{\bar{J}}_\tau\bar{u})_{\bar{\Omega}'}. \tag{30}$$

Substituting into (25) yields

$$\frac{d}{d\tau}\|\bar{u}\|_{\bar{\Omega}}^2 = 2\,\mathrm{Im}[(\bar{u}, D_\Delta\bar{u} + SAT_\Delta)_{\bar{\Omega}}]. \tag{31}$$

We continue by treating the remaining term of (31), related to D_Δ: This term should equal zero, just as the corresponding term in the continuous analysis. From the SBP relation in (19) we get

$$(\bar{u}, D_{2\xi}^{(\bar{\alpha}_1)}\bar{u})_{\bar{\Omega}'} = \bar{u}^* M_\xi^{(\bar{\alpha}_1)}\bar{u} + BT_{2\xi} \tag{32}$$

and

$$(\bar{u}, D_{2\eta}^{(\bar{\alpha}_2)}\bar{u})_{\bar{\Omega}'} = \bar{u}^* M_\eta^{(\bar{\alpha}_2)}\bar{u} + BT_{2\eta}. \tag{33}$$

Since M_ξ and M_η are positive semi definite $\mathrm{Im}[\bar{u}^* M_\xi^{(\bar{\alpha}_1)}\bar{u}] = 0$ and $\mathrm{Im}[\bar{u}^* M_\eta^{(\bar{\alpha}_2)}\bar{u}] = 0$. Hence the contribution from these second derivative terms to the discrete probability density is reduced to the boundary terms

$$\begin{aligned} BT_{2\xi} &= \bar{u}^*_{(\mathcal{E})} H_\eta \bar{\bar{\alpha}}_1 d_{\mathcal{E}}^\top \bar{u} - \bar{u}^*_{(\mathcal{W})} H_\eta \bar{\bar{\alpha}}_1 d_{\mathcal{W}}^\top \bar{u}, \\ BT_{2\eta} &= \bar{u}^*_{(\mathcal{N})} H_\xi \bar{\bar{\alpha}}_2 d_{\mathcal{N}}^\top \bar{u} - \bar{u}^*_{(\mathcal{S})} H_\xi \bar{\bar{\alpha}}_2 d_{\mathcal{S}}^\top \bar{u}. \end{aligned} \tag{34}$$

The SBP property of D_1 defined in (18) allows us to rewrite the mix derivative terms as

$$(\bar{u}, D_\xi \bar{\bar{\beta}} D_\eta \bar{u})_{\bar{\Omega}'} = -(D_\xi \bar{u}, \bar{\bar{\beta}} D_\eta \bar{u})_{\bar{\Omega}'} + BT_{\xi\eta}, \tag{35}$$

and

$$(\bar{u}, D_\eta \bar{\bar{\beta}} D_\xi \bar{u})_{\bar{\Omega}'} = -(\bar{\bar{\beta}} D_\eta \bar{u}, D_\xi \bar{u})_{\bar{\Omega}'} + BT_{\eta\xi}. \tag{36}$$

Since $(D_\xi \bar{u}, \bar{\bar{\beta}} D_\eta \bar{u})_{\bar{\Omega}'} = (\bar{\bar{\beta}} D_\eta \bar{u}, D_\xi \bar{u})^*_{\bar{\Omega}'}$, the contribution to the discrete probability density from these mix derivative terms is the boundary terms

$$\begin{aligned} BT_{\xi\eta} &= \bar{u}^*_{(\mathcal{E})} H_\eta \bar{\bar{\beta}} e_{\mathcal{E}}^\top D_\eta \bar{u} - \bar{u}^*_{(\mathcal{W})} H_\eta \bar{\bar{\beta}} e_{\mathcal{W}}^\top D_\eta \bar{u} \\ BT_{\eta\xi} &= \bar{u}^*_{(\mathcal{N})} H_\xi \bar{\bar{\beta}} e_{\mathcal{N}}^\top D_\xi \bar{u} - \bar{u}^*_{(\mathcal{S})} H_\xi \bar{\bar{\beta}} e_{\mathcal{S}}^\top D_\xi \bar{u}. \end{aligned} \tag{37}$$

Adding (32), (33), (35), (36) and the SAT_Δ defined in (24) yields

$$\mathrm{Im}[(\bar{u}, D_\Delta \bar{u} + SAT_\Delta)_{\bar{\Omega}}] = 0. \tag{38}$$

Equation (31) now reduces to

$$\frac{d}{d\tau}\|\bar{u}\|^2_{\bar{\Omega}} = 0. \tag{39}$$

Therefore the probability density is preserved and the scheme is time-stable. □

3.3. Time integration

It is well known that the time-scale of solutions to the Schrödinger equation is shorter than the length scale. Hence, small time steps are required for accurate solutions. For explicit schemes, the *Courant–Friedrichs–Lewy* (CFL) condition gives the requirement that the time step has to be proportional to h^2. One important application of our scheme is to simulate adiabatically deforming systems. In such systems, the frequency of the wave function is on a much shorter time-scale than the domain deformation. This type of systems requires long simulations, but the time step has to be adjusted to resolve the short time-scale of the wave function. Therefore, the choice of time integrator is crucial for efficient simulations of this type of problem.

The set-up with a time-dependent coordinate transformation gives a system of equations seen as a Schrödinger equation with a time-dependent Hamiltonian. For this problem type, the Magnus-Lanczos time integration scheme has shown to be competitive choice [18]. For the Magnus-Lanczos integrator the problem must be written on the form $\bar{v}_t = \mathcal{A}(t)\bar{v}$ where A is a skew symmetric matrix. The scheme derived in this work can be rewritten as a skew symmetric system by performing the change of variables $\bar{u} = H_{\xi\eta}^{1/2}\bar{\bar{J}}^{-1/2}\bar{q}$. If we denote the action of the scheme in (20) by $\mathcal{D}(t)$, i.e.

$$\bar{u}_t = \mathcal{D}(t)\bar{u}, \tag{40}$$

and apply the change of variables, we get

$$\bar{q}_t = \tilde{\mathcal{D}}(t)\bar{q}, \tag{41}$$

where $\tilde{\mathcal{D}} = H^{1/2}\bar{\bar{J}}^{-1/2}(\mathcal{D} + \bar{\bar{J}}_\tau/2)\bar{\bar{J}}^{-1/2}H^{-1/2}$. This $\tilde{\mathcal{D}}$ can be shown to be skew-symmetric by the same arguments used in the stability proof.

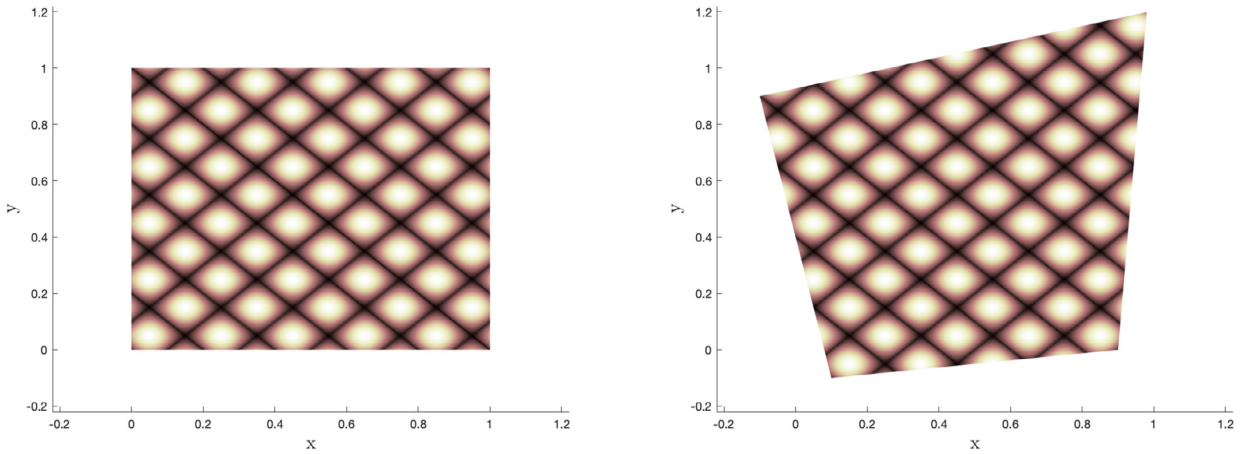

(a) Initial solution (b) End solution

Fig. 2. Real part of the analytical solution at the initial and final time of the convergence test.

In this work, the fourth order Magnus-Lanczos integrator presented in [19] is used. A drawback with the Magnus-Lanczos scheme is that it does not allow for a forcing term to be added to the system. In convergence test, presented in the following section, a forcing function is added at the boundary in order for the scheme to fulfil an analytical solution. In this case the Magnus-Lanczos scheme can not be used. Instead, the standard fourth order Runge-Kutta scheme is used with a step proportional to h^2. This is by no means an optimal time integrator but since long simulations are not required for the convergence test it is possible to use the fourth order Runge-Kutta scheme in this case. In practical applications, this constraint is not a limitation since we expect infinite potential walls which is equivalent to a homogeneous Dirichlet boundary condition at all boundaries.

4. Convergence study

For the Schrödinger equation on a moving quadrangular domain with homogeneous Dirichlet boundary conditions, no analytic solution to verify the convergence is known to the authors. Therefore, a manufactured solution is employed to verify the convergence properties of the scheme. The plane wave

$$\hat{u}_{ref}(t,x,y) = e^{i(10\pi x-(10\pi)^2 t)} + e^{i(10\pi y-(10\pi)^2 t)}$$

is chosen as the solution, which is the analytical solution to

$$\begin{aligned} &\hat{u}_t = i\Delta\hat{u}, && (x,y)\in\Omega(t), && t>0,\\ &\hat{u} = \hat{u}_{ref}(t,x,y), && (x,y)\in\partial\Omega(t), && t\geq 0,\\ &\hat{u} = \hat{u}_{ref}(0,x,y), && (x,y)\in\Omega(t), && t=0. \end{aligned} \tag{42}$$

The quadrangular domain deformation is prescribed by moving the coordinates of the corners along the following paths:

$$\begin{aligned} &\text{Lower left corner:} && x = 10t, && y = -10t.\\ &\text{Lower right corner:} && x = 1-10t, && y = 0.\\ &\text{Upper right corner:} && x = \cos(20t), && y = 1+\sin(20t).\\ &\text{Upper left corner:} && x = -10t, && y = 1-10t. \end{aligned} \tag{43}$$

The test is run until $t = 10^{-2}$ which corresponds to $\pi/2$ periods of the plane wave. The standard 4th order Runge-Kutta as time integration scheme is used. The initial condition $u_{ref}(0,x,y)$ and the analytical solution at the end time is shown in Fig. 2. The time step is chosen as $0.2h^2$. The convergence rate k is calculated as

$$k = \log\left(\frac{e_{N_2}}{e_{N_1}}\right) \Big/ \log\left[\left(\frac{N_2-1}{N_1-1}\right)^{1/2}\right], \tag{44}$$

where e_N is the l_2-error of the solution on a grid with N points in each spatial direction. The convergence rate and l_2 errors are shown in Table 1. The computed convergence rates agree with the theoretical result ($k=2$ for 2nd order $k=4$ for 4th order and $k=5$ for 6th order, see Remark 1).

Table 1
l_2 errors and convergence rates for the convergence test.

	2nd order		4th order		6th order	
N	$\log_{10}(e)$	k	$\log_{10}(e)$	k	$\log_{10}(e)$	k
25	0.23	-	-0.34	-	-0.41	-
51	-0.38	1.91	-1.49	3.63	-1.98	5.22
101	-0.98	1.98	-2.77	4.26	-3.75	5.87
201	-1.58	2.00	-4.00	4.07	-5.43	5.60
401	-2.18	2.00	-5.21	4.00	-6.97	5.12

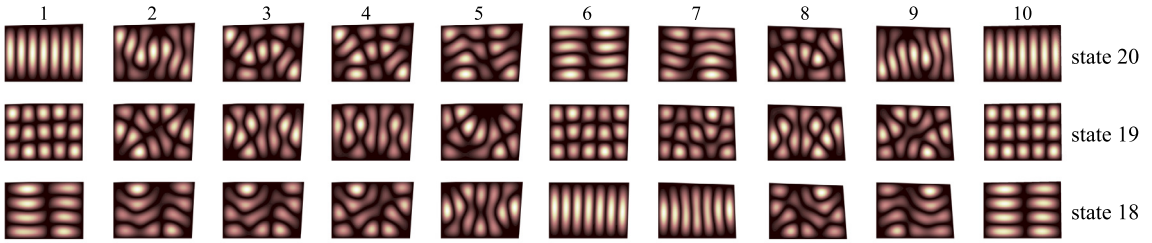

Fig. 3. Adiabatic evolution of eigenstate 18-20 when the upper right corner is encircling the diabolical point, $T_{end} = 100$.

5. Application

In this section, we apply our numerical method, which is designed for the problem of a quadrangular 2D domain, to the situation of one adiabatically moving corner. The eigenfunctions of the quadrangular domain have been studied by means of microwave cavity analogue experiments in [20–22]. By taking snapshots of the standing wave pattern for a sequence of boundary shapes, these experiments examined the behaviour of the Berry phase [4] in the vicinity of degeneracies of the normal modes. This phase shift corresponds to a sign change when taking certain normal modes around a diabolical point. The sign change was confirmed by assigning a sign locally to the wave and following this sign pattern in a continuous manner around the path in parameter space.

As a test of our method, we demonstrate how these Berry phases can be obtained in a fully quantum-mechanical setting by solving the time-dependent Schrödinger equation in this system.

The experiment of [20] considered the triply degenerate 18th - 20th normal modes of a rectangular quantum billiard with the side length ratio 1 to $\sqrt{3}$. To reproduce the results of [20] in the quantum-mechanical setting, we construct a computational domain with the lower left corner at $x = 0$, $y = 0$, the lower right corner at $x = \sqrt{3}$, $y = 0$ and the upper left corner at $x = 0$, $y = 1$. A diabolical point is formed for the upper right corner at $x = \sqrt{3}$, $y = 1$, for which the 18th - 20th energy eigenstates corresponding to the quantum numbers $(n_x, n_y) = (2, 4), (7, 1), (5, 3)$ are degenerated. For a quantum billiard of this box configuration the energy is $E_{n_x,n_y} \propto \frac{n_x^2}{3} + n_y^2$. Hence, it is easy to determine that the energy of the 18th - 20th state is equal to $13 \times E_g$, $E_g = E_{1,1}$ being the ground state energy of this configuration. The diabolical point is encircled by displacing the upper right corner and moving it along the elliptical path

$$(x_\theta, y_\theta) = (\sqrt{3}, 1) + a(\cos c, \sin c)\cos\theta + b(-\sin c, \cos c)\sin\theta \tag{45}$$

with parameter $0 \le \theta \le 2\pi$, and constants $a = 0.1023$, $b = 0.02313$, and $c = 0.4739$.

In order to capture the adiabatic behaviour the time-scale of the deformation has to be slow enough for the system approximately to remain in the eigenstate. Fig. 3 displays a simulation where the upper right corner has moved with constant speed along the ellipse in Eq. (45) for eigenstates 18-20. The simulation is run until $T_{end} = 100$. The velocity of the upper right corner is chosen such that the corner returns to its initial position at T_{end}. This figure displays snapshots of the probability density $|u(x, y, t)|^2$ when the upper right corner of the quantum billiard is at the positions shown in Fig. 4 along the elliptical path. It can be observed that the standing wave solution is modified as the corner moves along the ellipse, but approximately returns to the original state as the corner approaches its original position. For state 18 and 20 the solution has been subjected to a geometric phase shift of π. To visualise the phase shift, Fig. 5 shows the simulation in Fig. 3 but with the anti-nodes of the probability density coloured alternating in red and yellow. The colouring is following the changes of the state continuously as the upper right corner moves along the elliptic curve. A swap of the colours between position 1 and 10 indicates a Berry phase shift of π. Both this result and the intermediate states agree well with the results in [20].

To implement adiabatic evolution of the confined quantum particle, the boundary has to move slowly in comparison with the frequency of the wave function. Since two different time scales are present in this kind of evolution, efficient and accurate numerical methods are required. Thus, the method needs to be applicable for a wide range of time-scales, including adiabatic as well as non-adiabatic changes of the domain.

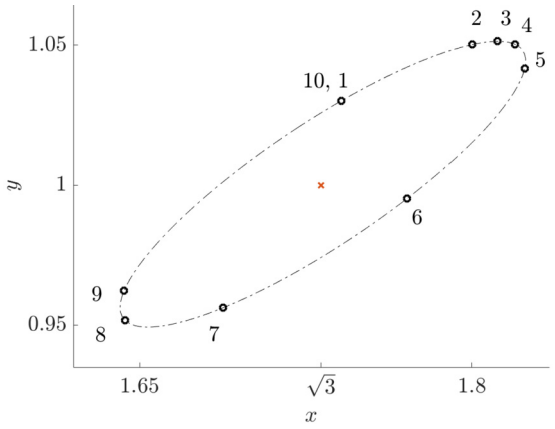

Fig. 4. Path of upper right corner. Note that the points 1 and 10 coincide.

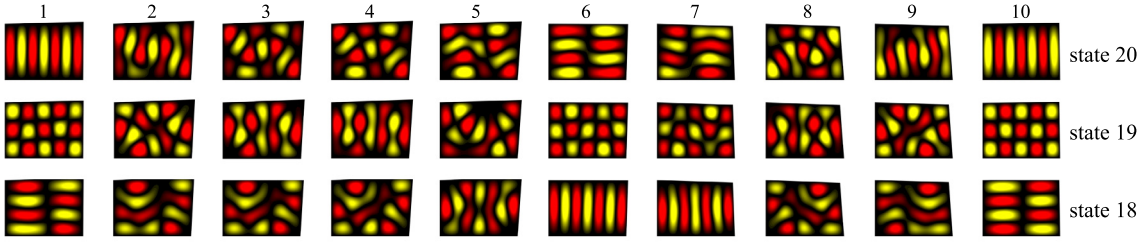

Fig. 5. Adiabatic evolution, coloured in order to detect geometric phase shift.

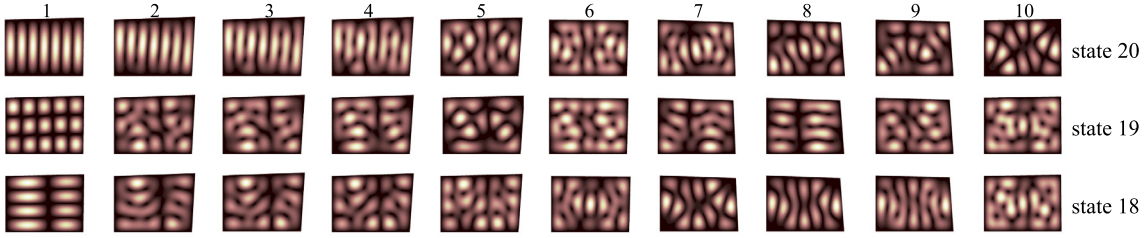

Fig. 6. Non-adiabatic evolution of eigenstate 18 - 20 when the upper right corner is encircling the diabolical point. $T_{end} = 10$.

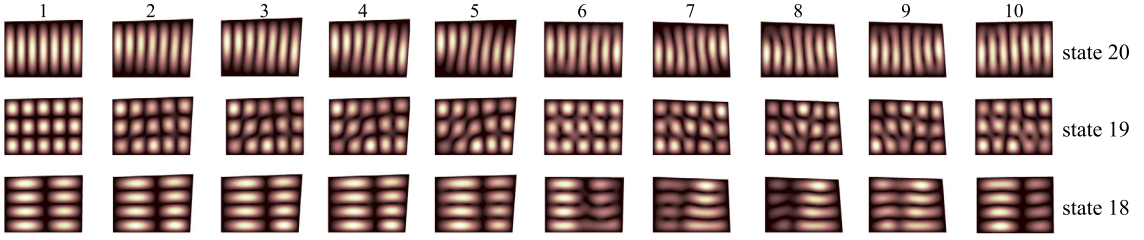

Fig. 7. Time evolution in the sudden approximation regime of eigenstate 18 - 20 when the upper right corner is encircling the diabolical point. $T_{end} = 0.1$.

We demonstrate in Figs. 6 and 7 that our method is qualitatively able to capture the dynamics at shorter, non-adiabatic time-scales. These simulations have the same set-up as the adiabatic one in Fig. 3 apart from that the corner moves with different velocities along the elliptical curve. In Fig. 6 the velocity is 10 times the velocity of the adiabatic simulation and in Fig. 7 the speed is 1000 times the speed in the adiabatic case. In the two cases, where the system is subjected to more rapid deformations than in the adiabatic simulation, mixing of the eigenstates occurs, which causes different physical effects. In particular, Fig. 7 shows that the wave pattern is almost unaffected under a rapid change. According to the sudden approximation (see e.g. [23]), being applicable to rapidly changing Hamiltonians, one expects that the time evolution operator is

close to the identity, which means that the probability density is expected to remain unchanged during the deformation. This indeed is consistent with our simulation.

The numerical experiments are run with 6th order SBP operators with $N_\xi = N_\eta = 60$. The fourth order Magnus-Lancsoz time integrator is used with the time step $0.1h$. For the Laczos iterations the error tolerance is set to 10^{-10}. In all cases, the numerical experiments are initiated with the upper right corner in point 1 at Fig. 4 with the corresponding eigenstate of this quantum billiard as initial condition.

6. Conclusions

In this paper, a provably stable high-order finite difference method for the time-dependent 2D Schrödinger equation on deforming domains has been derived by using the SBP-SAT framework. The domain deformation is treated by a time-dependent coordinate transformation that introduces a time-dependent variable coefficient and an additional term to the Schrödinger equation. The convergence properties of the scheme are verified by numerical experiment for 2nd, 4th and 6th order SBP operators. Further, a numerical experiment of a deforming quadrangular domain at different time-scales has been presented, which in the adiabatic limit demonstrates the existence of a non-trivial Berry phase. In the future, we aim to extend the discretisation to include external magnetic fields, as well as to the non-linear Gross-Pitavieski equation.

CRediT authorship contribution statement

Ylva Ljungberg Rydin: Conseptualization, Methodology, Software, Validation, Formal Analysis, Writing, Visulatzation. **Ken Mattsson:** Conseptualization, Methodology, Supervision. **Jonatan Werpers:** Conseptualization, Methodology, Software, Formal Analysis, Writing, Visulatzation. **Erik Sjöqvist:** Conseptualization, Writing, Visulatzation, Supervision.

Declaration of competing interest

The authors declare that they have no known competing financial interests or personal relationships that could have appeared to influence the work reported in this paper.

Appendix A. Supplementary material

Supplementary material related to this article can be found online at https://doi.org/10.1016/j.jcp.2021.110530.

References

[1] M.C. Gutzwiller, Chaos in Classical and Quantum Mechanics, Springer Verlag, New York, 1990.
[2] M.V. Berry, M. Wilkinson, Diabolical points in the spectra of triangles, Proc. R. Soc. Lond. Ser. A 392 (1984) 15–43.
[3] E.J. Heller, Bound-state eigenfunctions of classically chaotic Hamiltonian systems: scars of periodic orbits, Phys. Rev. Lett. 53 (1984) 1515–1518.
[4] M.V. Berry, Quantal phase factors accompanying adiabatic changes, Proc. R. Soc. Lond. Ser. A 329 (1984) 45–57.
[5] S. Abarbanel, A. Ditkowski, Asymptotically stable fourth-order accurate schemes for the diffusion equation on complex shapes, J. Comput. Phys. 133 (1997) 279–288.
[6] A. Bayliss, K.E. Jordan, B.J. Lemesurier, E. Turkel, A fourth order accurate finite difference scheme for the computation of elastic waves, Bull. Seismol. Soc. Am. 76 (1986) 1115–1132.
[7] J.S. Hesthaven, A stable penalty method for the compressible Navier-Stokes equations: III. Multidimensional domain decomposition schemes, SIAM J. Sci. Comput. 20 (1998) 62–93.
[8] S.K. Lele, Compact finite difference schemes with spectral-like resolution, J. Comput. Phys. 103 (1992) 16–42.
[9] S. De Rango, D.W. Zingg, A high-order spatial discretization for turbulent aerodynamic computations, AIAA J. 39 (2001) 1296–1304.
[10] D.C. Del Rey Fernández, J.E. Hicken, D.W. Zingg, Review of summation-by-parts operators with simultaneous approximation terms for the numerical solution of partial differential equations, Comput. Fluids 95 (2014) 171–196.
[11] M. Svärd, J. Nordström, Review of summation-by-parts-operators schemes for initial-boundary-value problems, J. Comput. Phys. 268 (2014) 17–38.
[12] A. Nissen, G. Kreiss, M. Gerritsen, High order stable finite difference methods for the Schrödinger equation, J. Sci. Comput. 55 (2013) 173–199.
[13] A. Nissen, G. Kreiss, M. Gerritsen, Stability at nonconforming grid interfaces for a high order discretization of the Schrödinger equation, J. Sci. Comput. 53 (2012) 528–551.
[14] S. Nikkar, J. Nordström, Fully discrete energy stable high order finite difference methods for hyperbolic problems in deforming domains, J. Comput. Phys. 106 (2015) 385–395.
[15] M. Almquist, I. Karasalo, K. Mattsson, Atmospheric sound propagation over large-scale irregular terrain, J. Sci. Comput. 61 (2014) 369–397.
[16] K. Mattsson, Summation by parts operators for finite difference approximations of second-derivatives with variable coefficients, J. Sci. Comput. 51 (2011) 650–682.
[17] M. Svärd, J. Nordström, On the order of accuracy for difference approximations of initial-boundary value problems, J. Comput. Phys. 218 (2006) 333–352.
[18] K. Kormann, S. Holmgren, H.O. Karlsson, Accurate time propagation for the Schrödinger equation with an explicitly time-dependent Hamiltonian, J. Chem. Phys. 128 (2008) 184101.
[19] M. Hochbruck, A. Ostermann, Exponential integrators, Acta Numer. 19 (2010) 209–286.
[20] H.-M. Lauber, P. Weidenhammer, D. Dubbers, Geometric phases and hidden symmetries in simple resonators, Phys. Rev. Lett. 72 (1994) 1004–1007.
[21] C. Dembowski, H.-D. Gräf, H.L. Harney, A. Heine, H. Rehfeld, W.D. Heiss, A. Richter, Experimental observation of the topological structure of exceptional points, Phys. Rev. Lett. 86 (2001) 787–790.
[22] B. Dietz, H.L. Harney, O.N. Kirillov, M. Miski-Oglu, Exceptional points in a microwave billiard with time-reversal invariance violation, Phys. Rev. Lett. 106 (2011) 150403.
[23] A. Messiah, Quantum Mechanics, Vol. II, North-Holland, Amsterdam, 1962, pp. 740–742.